Binding Studies on the *Neisseria* Opa Protein Interaction with Human CEACAM Receptor

Ji In Han

University of Virginia
Department of Chemistry

Research under the supervision of Dr. Linda Columbus

Spring 2018

Table of Contents

1. Abstract

Pathogenic *Neisseria* bacteria, which cause the diseases meningitis and increasingly antibiotic-resistant forms of gonorrhea, induce engulfment into diverse cell types by engaging their outer membrane opacity-associated (Opa) adhesin proteins with the host receptor, carcinoembryonic antigen-related cellular adhesion molecules (CEACAMs). A widely-studied class of CEACAM receptors, CEACAM1, is expressed in most immune cells, and interacts with Opa_{60}, an Opa protein variant. In addition to recognizing Opa_{60}, CEACAM1 binds itself homotypically. N-glycosylation of residues on the CEACAM1 Ig_V domain (nCEACAM1) has been shown to prevent homodimerization, which is necessary to study the Opa_{60}-nCEACAM1 interaction *in vitro*. The Opa_{60} binding interaction with N-glycosylated nCEACAM1 was investigated *in vitro* using surface plasmon resonance (SPR) spectroscopy. Additionally, binding conditions were optimized in order to improve immobilized Opa_{60} liposome surface regeneration and to reduce non-specific binding (NSB) to the streptavidin (SA)-coated SPR sensor surface. Significant reduction of NSB was achieved with the addition of 1% BSA to flow buffer. Initial binding studies suggest that a 1:1 steady-state kinetics model describes the wild-type Opa_{60} and GlcNAc-nCEACAM1 interaction, compared to a limited response from the HV-less (HV-) Opa_{60} control.

2. Introduction

2.1 Opa-CEACAM interaction

Neisseria meningitidis and *Neisseria gonorrhoeae* infect the human body to cause the globally infectious diseases meningitis and gonorrhea, respectively. Growing cases of multidrug antibiotic-resistant strains of *N. gonorrhoeae* renders treatment and eradication of the disease a severe public health challenge.[1-2] Gram-negative *Neisseria* induce phagocytosis into a wide variety of human cells, from macrophages and lymphocytes to epithelial cells, which are normally non-phagocytic. [3,4] Specifically, the interaction between opacity-associated (Opa) proteins of *Neisseria* and carcinoembryonic antigen-related cellular adhesion molecule (CEACAM) receptors on host cells initiate signaling events which eventually lead to engulfment into the host.[4] In addition to understanding Neisserial pathogenesis, Opa-CEACAM interactions have potential use as components of drug-delivery nanoparticles (NPs) that rely on site-specific targeting and uptake to improve the efficacy and safety of drug delivery.[5,6] The therapeutic effects of liposome delivery constructs depend on the binding of liposomes with specific receptors on the target surface[7], emphasizing the importance of studying the Opa-CEACAM binding profile.

Opa is phase-variably expressed on the outer membrane and consists of eight-stranded integral ß-barrels and four extracellular loops, three of which contain regions of high sequence variability between Opa variants, referred to as hypervariable (HV) and semivariable (SV) (Figure 1)[8]. The HV and SV regions of Opa_{60} engage the N-terminal immunoglobulin variable (IgV)-like domain of CEACAM1 (nCEACAM1) in interactions leading to phagocytosis and determine receptor specificity.[9-12] Through chimeric studies, it has been shown that both HV1 and HV2, but not SV, are required for CEACAM binding.[10] In other words, the lack of HV regions on Opa precludes the specific interaction between the two proteins. Although NMR studies on Opa_{60} structure have uncovered a wide-ranging ensemble of dynamic loop conformers[8], the mechanism of Opa-CEACAM binding is still under investigation.

As receptors responsible for cell adhesion and various signaling events, CEACAMs engage multiple other binding targets *in vivo*, including homotypic and heterotypic interactions with itself in diverse oligomeric states.[13] The nCEACAM1 residues that bind Opa_{60} and other targets are shown in Figure 2. Particularly, nCEACAM1 homodimerization has been described *in vitro*.[14,15] Although the affinity for Opa_{60}-nCEACAM1 binding (K_D = 1.6 nM[16]) has been found to be two orders of magnitude greater than that of

CEACAM1 homodimerization (K_D = 450 nM[13]), the CEACAM1 dimer prevails in unpublished Opa_{60}-nCEACAM1 *in vitro* binding studies. This tendency to dimerize poses a severe challenge to investigating the true Opa_{60}-nCEACAM1 binding conformations *in vitro*.

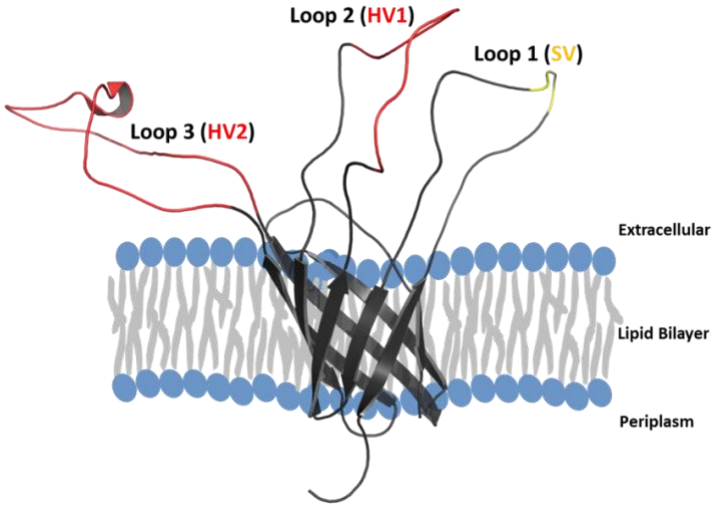

Figure 1. NMR-solved structure of a Opa_{60} (PDB: 2MLH[8]) membrane protein conformation. Opa_{60} engages CEACAM1 through hypervariable (HV) and semivariable (SV) loops in the extracellular matrix.

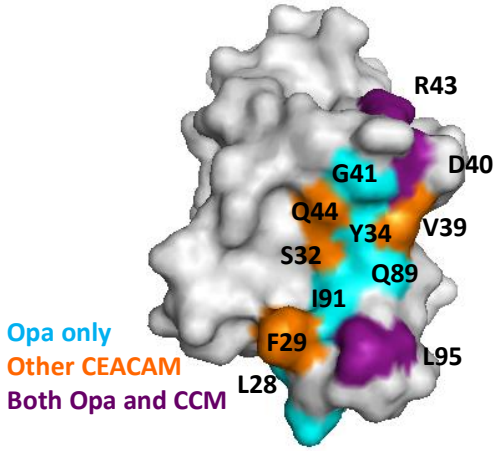

Figure 2. Structure of the N-terminal region of CEACAM1 (PDB: 2GK2[14]). nCEACAM1 interacts with two hypervariable loops on the extracellular side of Opa via residues shown in blue. The Opa-binding interface of nCEACAM1 also possesses residues that bind other CEACAM receptors shown in orange. Some residues bind both Opa and CEACAM (purple).[12]

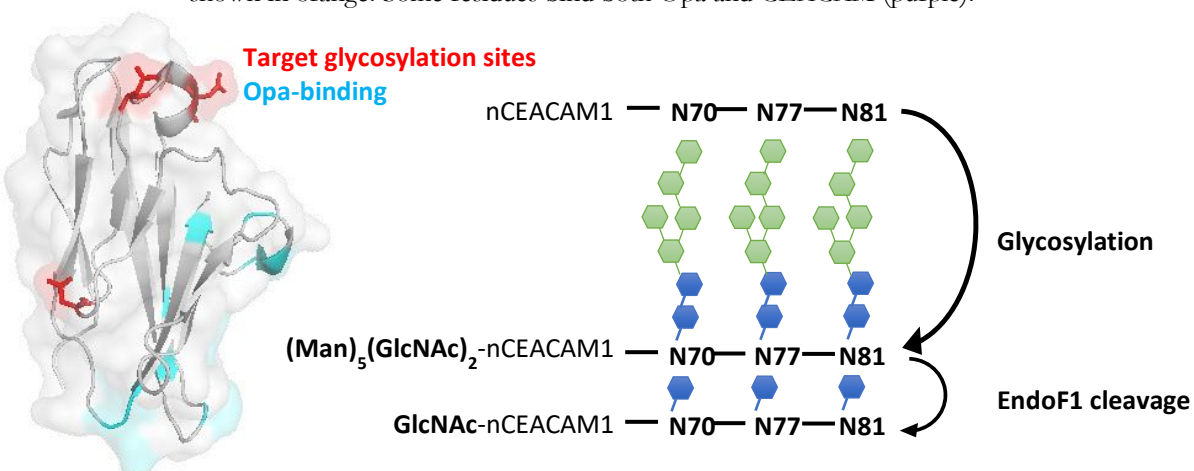

Figure 3. N-linked oligosaccharides are attached *in vivo* to CEACAM1 residues (red) outside of the Opa-binding site (blue) and may prevent formation of homodimers. A single glucose molecule remains after endoglycosidase F1 (EndoF1) cleavage of the oligosaccharide chain.

It should be noted that nCEACAM1 samples used in prior affinity and structural studies were engineered with a Glutathione S-transferase (GST) purification tag at the N-terminal domain and expressed in *E. coli*[16], thus lacking the post-transcriptional modifications that are characteristic of eukaryotic cells. Only recently has Zhuo et al. established a nCEACAM1 preparation method that mimics native glycosylation with the addition of N-acetylglucosamine (GlcNAc) at three asparagine residues at the nCEACAM1 interface that lies outside of the Opa_{60} binding site (Figure 3).[17] N-glycosylation reportedly inhibits nCEACAM1 homodimer formation even at high concentrations (e.g. 150 μM). However, whether this particular modification of CEACAM1 impacts the Opa-CEACAM1 binding *in vitro* is yet unknown.

This study aimed to characterize the behavior of minimally N-glycosylated nCEACAM1 in the presence of Opa_{60} folded into liposomes mimicking the native outer-membrane environment. Surface plasmon resonance (SPR) spectroscopy was used to obtain binding signals produced by the interaction between GlcNAc-nCEACAM1 and wild type Opa_{60} (WT) or a HV-less Opa_{60} construct (HV-). Comparison of the WT and HV- sensorgrams gave insight into the specific Opa_{60}/GlcNAc-nCEACAM1 interaction. Optimization of SPR experimental conditions involving regeneration of the Opa_{60} liposome surface and the flow system were necessary. Unlike HV-, WT produced a significantly larger GlcNAc-nCEACAM1 binding signal that also fits a 1:1 model as expected. These initial observations merit further screening of the effect of optimized conditions for different concentrations of GlcNAc-nCEACAM1 in order to obtain accurate kinetic parameters.

2.1 Surface Plasmon Resonance

Optical biosensors are commonly used to determine association and dissociation kinetics of macromolecular interactions due to the advantages of being label-free and highly sensitive.[18,19] Surface plasmon resonance (SPR) is one technique which elucidates the binding of small analyte to target biomolecular ligands immobilized on a metal surface in real-time.[20] Protein-protein interactions can be determined using the change in refractive index and thickness of the protein ligand-immobilized metal interface as a result of analyte binding.[21] SPR utilizes high-affinity interactions to generate the protein-immobilized surface, including antibody capture, streptavidin (SA)-biotin, and covalent amine coupling among other methods.[22,23] Of specific interest is the reversible, high-affinity (K_D = 40 fM), non-covalent biological interaction between SA and biotin.[24,25] SA-biotin technology is widely applied in solid-phase biochemical techniques, including affinity purification and biosensor chip assays (SPR and bio-layer interferometry), in which biotin is covalently linked to the biomolecule of interest.[26] Thus, a biotin-linked protein of interest opens novel possibilities for efficient purification and characterization.

SPR utilizes the generation of surface plasmons at the interface between inert, conducting metal (usually gold or silver) and a positive dielectric layer (ligand-binding surface).[20] Surface plasmons are electromagnetic (EM) oscillations that propagate between these two surfaces and are generated upon a specific transfer of light energy to the free conducting electrons of the metal. Propagation of surface plasmons emits an EM field, which decays evanescently into both surface mediums by distance. Dampening of this "evanescent field" in the metal, but not in the binding medium, causes shorter decay into the metal than into the binding medium. This event lends SPR its sensitivity to changes in optical properties at the binding surface, most often measured as changes in refractive index.[20]

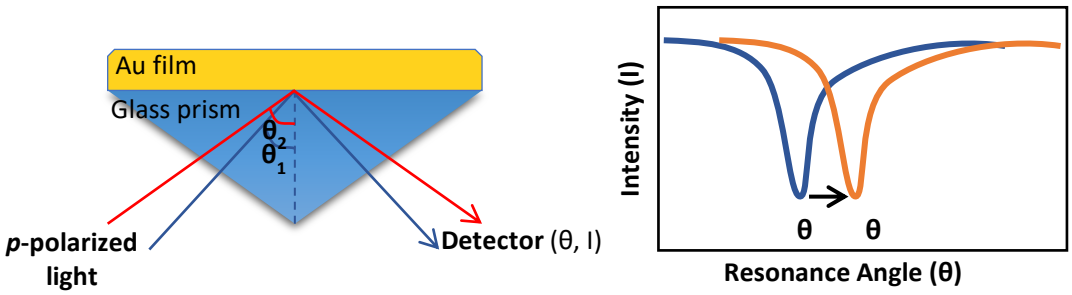

Figure 4. Kretchmann configuration detects the change in refractive index at the gold surface.

In the traditional Kretchmann configuration, *p*-polarized light achieves total internal reflection from the bottom of a gold-coated glass prism (Figure 4). Surface plasmon resonance occurs when incident photons of the same momentum as plasmons become absorbed, detected by a dip in intensity.[20] A simplified dispersion function, β, based on the Drude model[20] describes the relationship between the angular frequency, ω, and the surface plasmon wavevector along the metal-binding interface, where c is speed of light in vacuum, ε is permittivity and M and B are metal and binding surfaces, respectively:

$$\beta = \frac{\omega}{c}\sqrt{\frac{\varepsilon_M \varepsilon_B}{\varepsilon_M + \varepsilon_B}} \qquad (1)$$

Equation 1 relates to the evanescent field wavelength along the M/B interface. Due to dampening along the metal, small changes in refractive index are observed and detected as the change in angle of resonance.[20]

Since commercial availability of SPR using the Kretchmann configuration, alternative SPR systems have been developed, including localized SPR (LSPR).[28,29] Instead of the bulk metal surface involved in traditional SPR, LSPR utilizes novel metal nanoparticles (NPs), which strongly absorb in the UV-Vis region upon generation of surface plasmons and the evanescent field.[27,30] LSPR sensitivity also arises from the evanescent field at the binding surface[27], but change is detected by absorbance peak (nm) instead of incident angle. Equation 2 relates the collective optical properties of the binding medium local to the NPs, which determine the wavelength absorbed, where $\Delta\lambda_{max}$ is the wavelength shift response, m is the refractive index sensitivity, Δn is the change in refractive index induced by an adsorbate, d is the effective adsorbate layer thickness, and l_d is the electromagnetic field decay length[27]:

$$\Delta\lambda_{max} = m\,\Delta n\left(1 - e^{-2d/l_d}\right) \qquad (2)$$

Another significant feature of LSPR is the short decay length of the evanescent field decay, reducing the sensitive decay length to around 20-40 nm (compared to 100 nm for traditional SPR).[30] Thus, a localized field more closely detects changes in molecular binding, while limiting detection of changes due to non-ideal effects like bulk refractive index and temperature.

Analyte binding to immobilized ligand produces a binding signal as shown in Figure 5. In order to obtain kinetic constants, the association and dissociation phases of SPR sensorgrams are fitted to a kinetic model. Given the binding event,

$$A + B \underset{k_{off}}{\overset{k_{on}}{\rightleftharpoons}} AB \qquad (3)$$

the equilibrium dissociation constant, K_D, is determined from the association rate, k_{on}, and dissociation rate, k_{off}, as such:

$$K_D = \frac{k_{off}}{k_{on}} = \frac{[A][B]}{[AB]} \qquad (4)$$

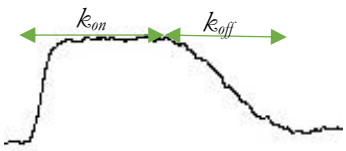

Figure 5. The association and dissociation phases on a model SPR sensorgram with analyte injection.

3. Methods

3.1 Expression and purification of Opa_{60}

Both WT and HV- Opa_{60} proteins were prepared by the same method. The HV- construct, which replaced each HV region with a 7-residue Ser-Gly repeat chain, was provided by Jason Kuhn in the Columbus Laboratory. Opa_{60} WT and HV- each were subcloned into the expression vector (pET28b) with an N-terminal His_6 tag for purification. Plasmids were transformed into *E. coli* BL21(DE3). An overnight culture was grown in LB medium supplemented with kanamycin (LB-Kan) at 37 ºC and 225 rpm. The culture was used to inoculate fresh LB-Kan (1 L) at 37ºC and 225 rpm until an OD_{600} of 0.6-1.0 (log phase) was reached. Expression was induced into inclusion bodies with 1 mM isopropyl-β-thio-D-galactoside for 4 h under the same conditions. Cells were harvested via centrifugation at 12000g and 12 ºC for 30 min.

Cells were lysed by microfluiding at 4 ºC after resuspension in lysis buffer (50 mM Tris pH 8.0 and 150 mM NaCl) with added protease inhibitor. Cell debris from the lysate was removed via centrifugation at 12000g and 12ºC for 30 min. Opa_{60} was extracted from the inclusion bodies by resuspending pellet in lysis buffer with the addition of 8 M urea overnight at room temperature and centrifuging again at 12000g and 12ºC for 30 min. For Opa_{60} purification, Co^{2+}-immobilized metal affinity chromatography (IMAC) column containing Chelating Sepharose Fast Flow resin (GE Healthcare) was equilibrated with lysis buffer. The soluble fraction (30 mL) was flowed through the IMAC column and washed with two 15 column volumes (CV) of wash buffer (20 mM phosphate, pH 7.8, 150 mM NaCl, 20 mM imidazole, and 8 M urea), followed by two 5 CV elutions (wash buffer with 680 mM imidazole). The eluted protein fraction (supplemental Figure 1) was concentrated (molecular weight cut-off (MWCO) = 10 kDa) to 2-5 mg/mL and stored in -20 ºC until use.

3.2 Refolding Opa_{60} into liposomes

The method for preparing Opa_{60} liposomes was adapted from Dewald et al.[31] Chloroform-dissolved 1,2-didecanoyl-*sn*-glycero-3-phosphocholine ($diC_{10}PC$) was dried under a continuous stream of nitrogen for 2 h minimum, resuspended into borate buffer (10 mM sodium borate, pH 12, 1 mM EDTA), and sonicated with a 1/8" micro tip (model Q500, Q Sonica) for 30 min at 40% amplitude and 4ºC. 8 M urea was added to the $diC_{10}PC$ suspension. 2-5 mg/mL Opa_{60} protein (1.5 mg of Opa_{60} WT and 1.25 mg of Opa_{60} HV-) was slowly stirred into lipid in 20 µL aliquots, yielding a molar lipid/protein ratio of 1160:1. The folding reaction proceeded at 37°C for 3 full days and was confirmed by a lower apparent MW shown in SDS-PAGE (supplemental Figure 2). Folded proteoliposomes were harvested via ultracentrifugation at 142,400 g and 10°C for 2 h. The Opa_{60} pellet, containing <20% of the initial $DiC_{10}PC$, was resuspended with a new lipid mixture in 30 mM Tris, pH 7.3, and 150 mM NaCl and pulse sonicated with a 1/8" micro tip for 20 min (30 s on/off) at 45% amplitude and 4ºC. The latter lipid mix was comprised of 65 mol% 1,2-dimyristoyl-*sn*-glycero-3-phosphocholine (DMPC), 17.5 mol% 1,2-dimyristoyl-*sn*-glycero-3-phospho-(1'-rac-glycerol) (DMPG), 17.5 mol% cholesterol, and 1 mol% biotinylated 1,2-dimyristoyl-sn-glycero-3-phosphoethanolamine-N-[methoxy(polyethylene glycol)-2000] (DMPE-PEG 2000). The final amount of DiC10PC present and the molar lipid/protein ratio were approximately 1 mol% and 234:1, respectively. The liposomes were then extruded 10 times at 25°C through 100 nm polycarbonate filters to reduce polydisperity and to obtain a size-homogenized sample.

3.3 Expression and purification of GlcNAc-nCEACAM1

The method for nCEACAM1 expression into mammalian HEK293S GnTI$^-$ cells was adapted from Zhuo et al.[17] In brief, HEK293S, which produces primarily $(Man)_5$-$(GlcNAc)_2$ glycosylation to target N-sites, was maintained at 0.5–3.0 × 10^6 cells/mL in FreeStyle™ 293 expression media (Thermo Fisher Scientific) in a humidified CO_2 platform shaker incubator at 37ºC. A codon-optimized NCEACAM1 construct – followed by a His_8 tag, AviTag, GFP, and tobacco etch virus (TEV) protease cleavage site – was subcloned into the expression vector (pGEn2) and provided by the Prestegard Lab (Athens, GA). Prior to transfection, cells were resuspended to approximately 2.5 × 10^6 cells/mL in fresh 9:1 (v/v) mixture of FreeStyle™ and EX-CELL® 293 serum-free (Sigma) media. To transfect cells, 4 μg/mL NCEACAM-pGEn2 plasmid DNA and 9 μg/mL of polyethyleneimine were directly added to the suspension culture. 2.2 mM valproic acid and 125mL of fresh 9:1 FreeStyle and EX-CELL media were added to cultures 24 h post-transfection. After 5 days of protein production at 37 °C, the cells were removed via centrifugation at 1200 rpm and 4ºC for 20 min.

A gravity-flow Co-IMAC loaded with supernatant was washed with 150 mL of Buffer A (20 mM HEPES, pH 7.2, 300 mM NaCl, 20 mM imidazole) and eluted with 150 mL Buffer B (25 mM HEPES, pH 7.0, 300 mM NaCl, 300 mM imidazole). Protein elution was concentrated to 1 mg/mL (MWCO = 10 kDa) and treated with endoglycosidase F1 (EndoF1) and TEV protease for 24 h while dialyzing to 20 mM HEPES, pH 7.0, 100 mM NaCl, 10% glycerol. Cleaved GlcNAc-nCEACAM1 was further purified by BioLogic Duoflow fast protein liquid chromatography (FPLC) system (Bio-Rad). Fractions corresponding to discrete elution peaks were analyzed by SDS-PAGE (supplemental Figure 3), and those containing the cleaved form were pooled and concentrated. The final GlcNAc-nCEACAM1 sample containing the monomer (analyzed by SEC-MALS) was provided by Marissa Keiber in the Columbus Lab.

3.4 SPR multicycle kinetic experiment

All SPR experiments were run on OpenSPR (Nicoya Life Sciences), an SPR instrument which uses LSPR principles. Before experimentation, the SA sensor chip (Nicoya Life Sciences) was rinsed with ddH_2O, dried under nitrogen, and primed in the SPR flow cell with flow buffer (1x PBS: 10 mM Na_2HPO_4, 1.8 mM KH_2PO_4, pH 7.4, 137 mM NaCl, 2.7 mM KCl). All samples were diluted and carried through the flow cell in the flow buffer. 300 mM Opa_{60} WT and HV- liposomes with biotinylated DMPE-PEG (2000) were immobilized to the SA surface at a speed of 20 μL/min. Prior to binding analyte, the Opa_{60}-immobilized surface was regenerated three times with 30 s injections of the regeneration buffer (10 mM NaOH) at 150 μL/min. Randomized injection cycles of five GlcNAc-nCEACAM1 concentrations (9 nM, 27 nM, 81 nM, 273 nM, 729 nM) and blank flow buffer were performed in triplicates, with one set discarded due to injection error. All analyte injections were performed at 30μL/min. Regeneration buffer was injected once between each analyte binding cycle for 30 s at 150 μL/min in order to recover the Opa_{60}-immobilized surface.

All analyte binding curves were processed using TraceDrawer software and were corrected by subtracting the flow buffer injection signal. The results were analyzed with a steady-state affinity binding model by fitting a plot of wavelength binding signal (nm), against GlcNAc-nCEACAM1 concentration. The steady-state analyte binding level signal is the relative wavelength calculated 10 s before injection stops.[32]

3.5 SPR regeneration scouting

300 nM Opa_{60} WT liposomes were immobilized and regenerated as done previously. Flow buffer and speed were also kept the same. Four ionic buffers (0.5 M NaOH, 1 M NaOH, 2 M $MgCl_2$, and 1 M $MgCl_2$) were sequentially used to regenerate the proteoliposome surface after a 100 nM GlcNAc-nCEACAM1 injection cycle. Scouting was conducted a single chip, in order of increasingly harsh conditions with the exception of

1 M $MgCl_2$, which had to be adjusted from 4 M after observing the regenerative effects of the 2 M $MgCl_2$. The baseline and analyte response signal, marked by 10 s before dissociation, were measured before surface exposure to any regeneration (control) and *after* each regeneration cycle. The baseline reached after each regeneration cycle was plotted relative to the signal generated by the control baseline. The analyte binding response after regeneration was plotted relative to the cycle's baseline. Relative baseline and analyte response were combined against cycle order on one plot.

3.6 SPR flow buffer optimization

Five different flow buffers were used to inject 100 nM GlcNAc-nCEACAM1 onto an empty SA surface, not immobilized with Opa_{60}. Buffer components commonly used to prevent nonspecific binding were added to the original PBS flow buffer: 200 mM NaCl, 250 mM NaCl, 1% BSA, and 1% BSA plus 250 mM NaCl. Analyte injection and regeneration cycles were done in triplicates for each flow buffer, under the same conditions as previously described.

The WT and HV- binding signals with 100 nM GlcNAc-nCEACAM1 produced in 1% BSA PBS flow buffer were compared to those produced in normal PBS. These sensorgrams were processed using a double referencing approach, in which the Opa_{60}-nCEACAM1 binding signals obtained were first subtracted from the control surface curve (sensor-nCEACAM1), followed by subtraction from the flow buffer injection cycle (buffer-Opa_{60}). All future kinetic experiments will be processed using this method.

4. Results & Discussion

4.1 Initial kinetic binding experiment

The SPR sensorgrams obtained from the multicycle kinetics experiment resulted in significantly different N-glycosylated CEACAM1 binding signals between Opa_{60} WT and HV- liposomes. The same amount of Opa_{60} was used, allowing comparison between the two sensorgrams shown in Figure 6.

While the differences between low concentrations of GlcNAc-nCEACAM1 (9nM and 27 nM) were indiscernible, the upper range produced variable signals. Because the affinity constant of nCEACAM1 homodimerization was 450nM, 720 nM GlcNAc-CEACAM1 above the threshold was expected to dimerize and produce a similar binding curves for WT and HV-. However, the binding signal was greater for WT than HV-, suggesting possibilities that glycosylation does prevent nCEACAM1 homodimerization or that the homodimer still retains the ability to bind Opa_{60}. At 243 nM GlcNAc-nCEACAM1, almost two-fold difference is seen, with the HV- binding signal greater than WT. The pronounced difference in binding signal may have been due to nonspecific binding of monomeric or dimeric nCEACAM1 to the liposome surface, Opa_{60} HV- β-barrel, or the polar residues (Gly-Ser repeats) that replaced the HV region. The gradual increase in slope after initial association indicates accumulation of NSB.[32] Although the difference produced by 81 nM GlcNAc-nCEACAM1 interaction with HV- and WT was expected, the significance was uncertain because protein-protein interaction signals in the low-concentration range can be greatly affected by buffer components.[32]

Global curve-fitting was attempted in order to obtain association and dissociation binding profiles of the Opa_{60} WT/GlcNAc-nCEACAM1 and Opa_{60} HV-/GlcNAc-nCEACAM1 interactions. Fitting to various 1:1 or 1:2 binding models (TraceDrawer) did not give satisfying results, which was not likely due to abnormal binding characteristics but rather due to limitations in experimental design. Signals were manually fit using steady-state affinity determined as described previously. As seen in Figure 7, accurate kinetic parameters could not be determined due to incomplete binding data on useful [GlcNAc-nCEACAM1]

points. Moreover, non-hyperbolic shape of the Opa_{60} binding curves again indicated the need to optimize SPR conditions before pursuing further binding studies.

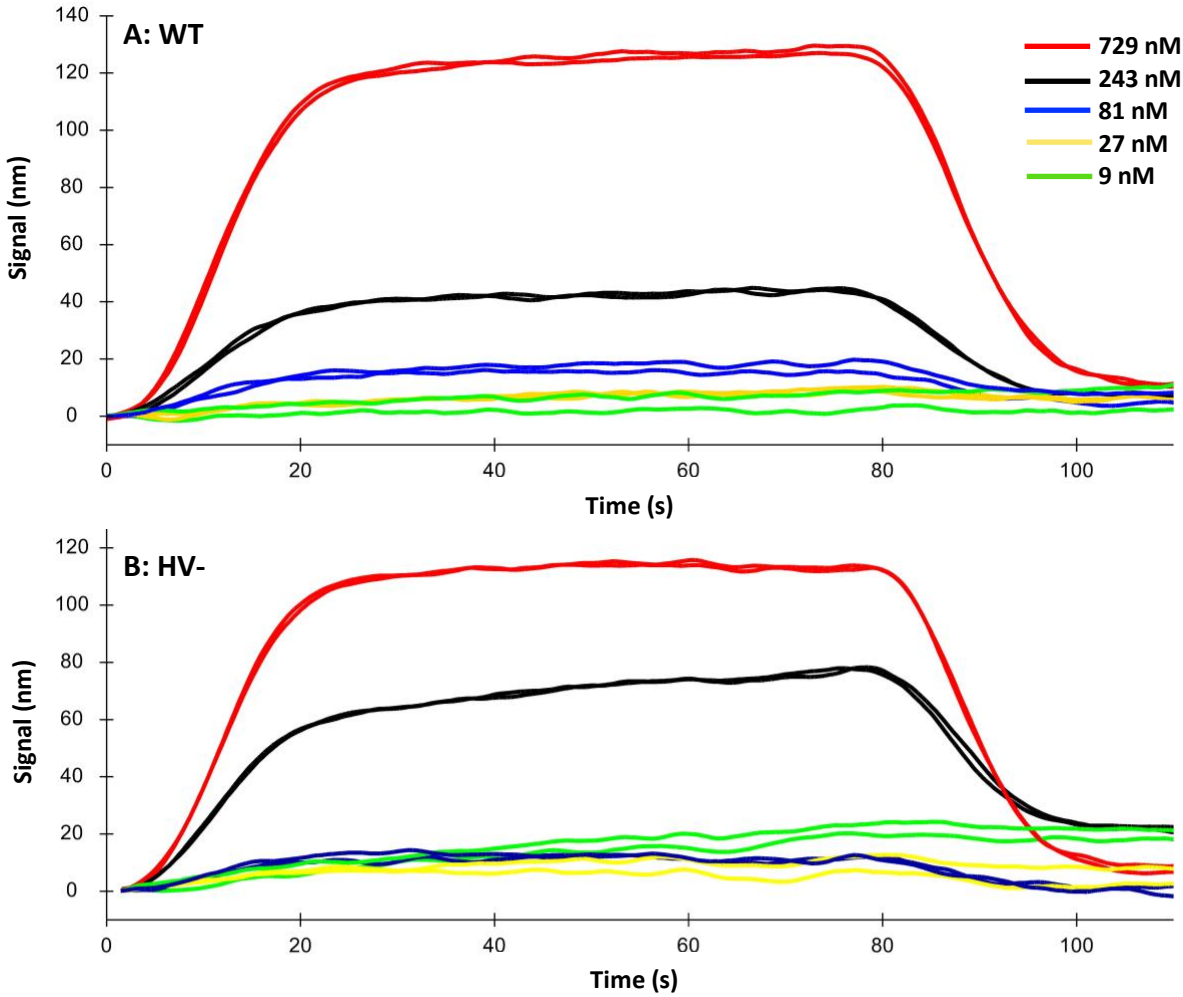

Figure 6. SPR sensorgrams of multicycle kinetics experiments with 300 nM (A) WT and (B) HV- Opa_{60} liposome and five concentrations of GlcNAc-nCEACAM1 ranging from 9 nM to 729 nM.

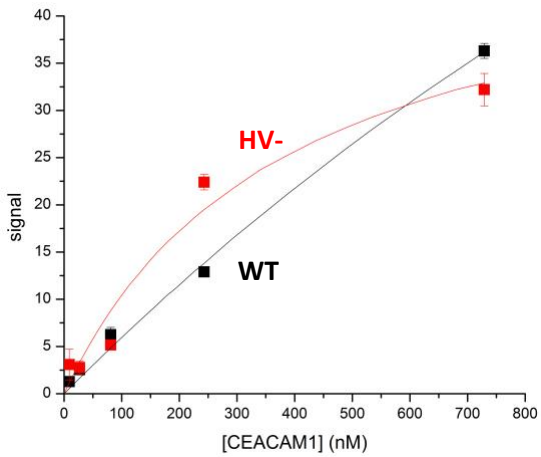

Figure 7. Steady-state affinity curves corresponding to the initial sensorgram shown in Figure 6. WT (black) and HV- (red) Opa_{60} liposomes injected with GlcNAc-nCEACAM1 are shown in the bottom and top curves, respectively. Error bars indicate the standard deviation across two trials. Optimization and more [CEACAM1] data points are needed in order to obtain accurate kinetic parameters.

4.2 Regeneration Scouting

The high observed off rate (approximated as the large negative slope during dissociation) for both WT and HV- sensorgrams suggested the loss of ligand activity, or ability to reproduce the same response level for the same CEACAM1 analyte. The 10 mM NaOH regeneration buffer used for the multicycle kinetics experiment was deemed too abrasive to use with negatively charged proteoliposomes. In high pH, immobilized liposomes that are permeable to OH^- ions may have been disrupted due to sudden excess of negative charge[33], possibly resulting in repulsion or influx of OH^-.[34] Additionally, fluorescent studies on liposomal drug retention have suggested pH-dependence of the intraliposomal microenvironment.[35] Thus, a new set of ionic regeneration buffers at neutral pH were scouted for efficacy, mainly removal of the bound analyte while maintaining activity of the immobilized ligand (Figures 8 and 9).[36]

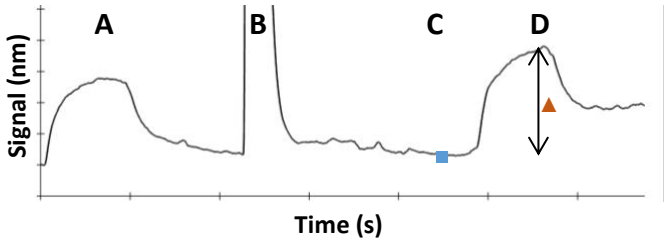

Figure 8. Sensorgram of a regeneration cycle (B-D). After regeneration (B) of the previous GlcNAc-nCEACAM1 injection (A), the signal to the original unbound ligand-baseline (C, blue marker) and analyte response (D, orange marker) should remain constant after an ideal regeneration.

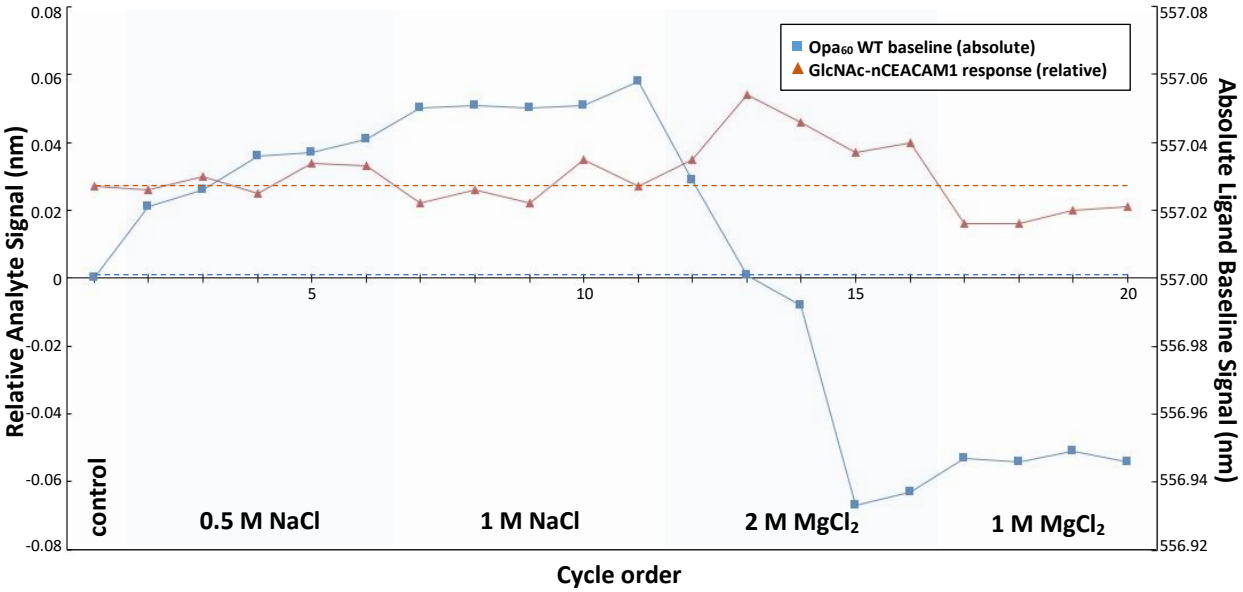

Figure 9. Scouting for regeneration capacity of ionic buffers. The effect of each regeneration on removing bound analyte and maintaining ligand activity was indicated by proximity to the baseline of the unregenerated Opa_{60} WT (control) surface and its relative analyte response, respectively. Cycles subsequent to the control response should produce signals close to the respective dotted lines.

A gradual increase in baseline was observed for regeneration with NaCl, indicating that some analyte remained bound. Regeneration with $MgCl_2$ buffers resulted in decrease in baseline, which was acceptable because, unlike NaCl, there was certainty that analyte has been completely removed. However, the relative baseline alone does not describe the effect of $MgCl_2$ on ligand binding capacity, and the analyte response was analyzed. The difference from control GlcNAc-CEACAM1 injection signals for 0.5 M NaCl, 1 M NaCl, 2 M $MgCl_2$, and 1 M $MgCl_2$ ranged within 25%, 30%, 100%, and 40%, respectively. Although use of 0.5 M NaCl buffer may be acceptable in short experiments with small number of cycles, the unbound ligand

surface available will likely become occupied with the target analyte towards the end of longer kinetic experiments requiring multiple analyte concentrations and repetitions. For 1 M $MgCl_2$, previous injections of the harshest condition, 2 M $MgCl_2$, likely affected the immobilized Opa_{60} liposomes over several cycles. Although analyte response in 1 M $MgCl_2$ decreased by almost 40% compared to the control, there was a small deviation of 8% between the buffer cycles' relative analyte response levels, while other buffers cycles ranged from 13% to 26%. Thus, from this particular experiment, 1 M $MgCl_2$ was chosen as the optimal regeneration buffer due to its baseline signal and consistent analyte response.

Due to the hypervariable nature of the HV loop sequences and unknown Opa_{60} bound structure, this trial-and-error approach to regeneration scouting had to be used to find the appropriate conditions to remove GlcNAc-nCEACAM1 analyte. nCEACAM1, however, *is* known to bind Opa proteins through mostly hydrophobic (L28, L95, Y34, I91) and polar (Q89, G41) residues, in addition to the R43 and D40 residues that may engage in ionic or other interactions with parts of the HV or SV loops. Because Opa is folded into liposomes that could be destabilized by surfactants, common hydrophobic regeneration buffers (e.g. < 0.5% SDS) that may have been effective in interrupting this binding could not be scouted.

4.2 Flow buffer optimization and preliminary screening of double-referencing method

For similar reasons, the flow buffer additions chosen to prevent non-specific binding to the SA sensor were limited to ionic (NaCl) and neutral (BSA) molecules instead of detergents such as Tween-20 or SDS. As expected, injections flown in unmodified PBS produced the highest signal and corroborated the need to further optimize the initial experimental conditions. Additions of 200 mM NaCl, 250 mM NaCl, and 1% BSA/250 mM NaCl produced similar sensor/GlcNAc-nCEACAM1 binding characteristics, all around 20 nm signal. Out of the five flow buffers tested, the addition of 1% BSA produced the lowest false binding signal (and no signal at 80-100 s of association) upon injection of 100 nM GlcNAc-nCEACAM1.

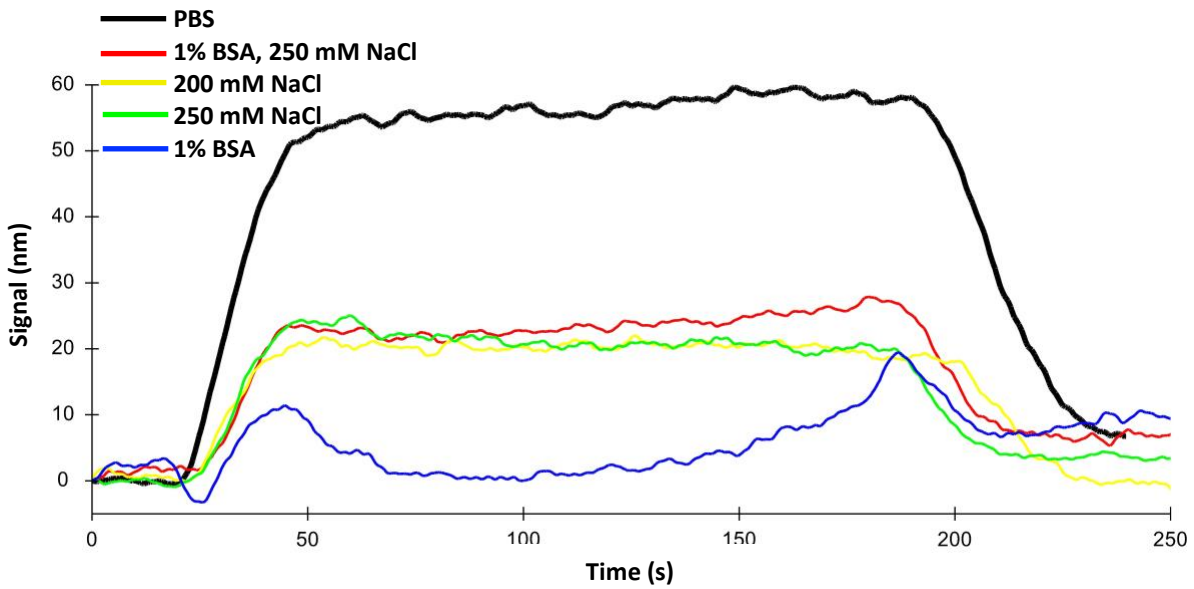

Figure 10. Addition of salt and globular bovine serum albumin (BSA) protein to PBS flow buffer significantly reduced NSB interactions between 100 nM GlcNAc-nCEACAM1 analyte and empty SA sensor chip. Although maximum reduction in NSB was achieved using 1% BSA (blue), mass transport limitation and the resulting irregular curvature may pose challenges to double-referencing (subtracting buffer and sensor signals).

The specific binding characteristics in 1% BSA-PBS as flow buffer were investigated for future experiments. Because the double-referencing method requires curve subtraction, preliminary data was processed for

sensorgrams obtained from 100 nM GlcNAc-nCEACAM1 injections over Opa_{60} WT and HV- in normal PBS and in 1% BSA. The resulting curves in Figure 11 display significant differences between the flow buffers used as well as between WT and HV-.

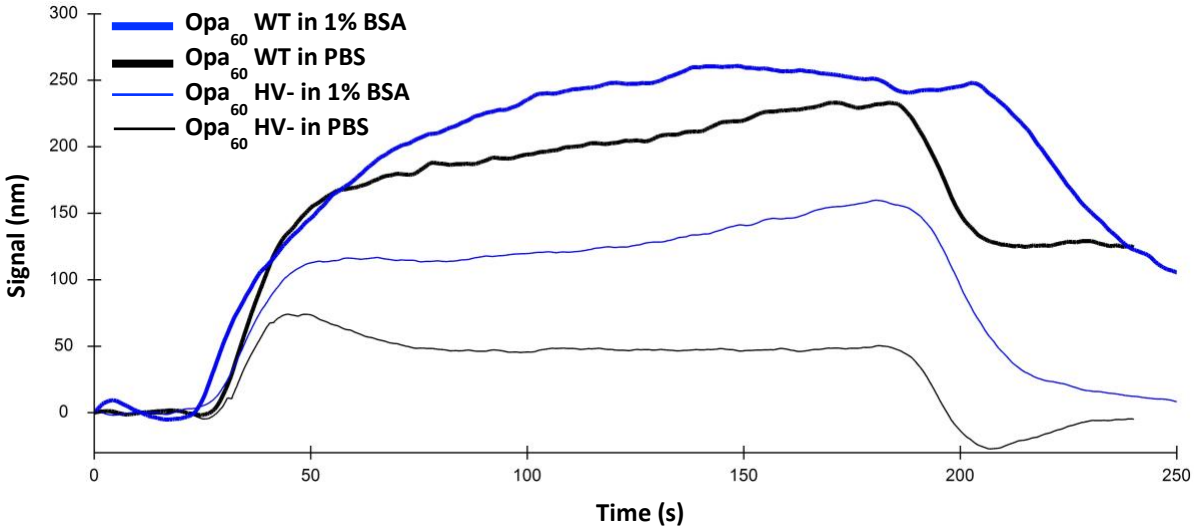

Figure 11. Opa_{60} WT (bolded) and HV- (regular) binding signals with 100 nM CEACAM1 in regular PBS (black) and 1% BSA PBS (blue) were referenced against sensor-CEACAM1 NSB signals shown in Figure 14. Both WT and HV- produced higher CEACAM1 binding signals in the presence of 1% BSA, whereas WT and HV- produced lower CEACAM1 signals overall but displayed expected large difference in response.

Although the subtracted curves in 1 % BSA (blue) were expected to be higher than in normal PBS (black) based on results of Figure 10, the difference between the HV- curves was greater than the difference explained by sensor-GlcNAc-nCEACAM1 NSB. For example, at 125 s, the WT signals (bold) differ by approximately 50 nm, which is the difference between the empty sensor signals produced in the two flow buffers. For HV-, however, the difference at the same injection point is almost two-fold. This could partly be explained by the lack of HV- loops, which are highly flexible in solution. HV loop dynamics or just the mere presence of extracellular amino acid residues could have prevented nonspecific interactions between globular BSA and the hydrophobic transmembrane ß-barrel embedded in the liposome. Alternatively, NSB between GlcNAc-nCEACAM1 and BSA, which is absent in PBS flow buffer experiments, offers an alternative explanation of the increased HV- signal in the 1% BSA system only. The availability of hydrophobic residues on both proteins may have allowed interaction

Most noticeably, WT/GlcNAc-nCEACAM1 binding (bolded lines, top) produced much slower dissociation trends than the initial sensorgram observed in Figure 6, with a signal difference of almost 100 nm at 250 s compared to both HV- signals (thin lines, bottom). In 1% BSA only, the WT binding signal (bold, blue) was successfully fitted to a 1:1 hyperbolic binding mode (supplemental Figure 4). From this information, it can be inferred that GlcNAc-nCEACAM1 retains the ability to interact with Opa_{60} WT in liposomes. Whether minimal N-glycosylation prevents homodimerization of nCEACAM1 (K_D = 450 nM) is uncertain, however, due to the lack of optimized data on concentrations of GlcNAc-nCEACAM1 above 100 nM.

5. Future Directions

Although the double-referenced WT in optimized flow buffer displays large improvement in binding signal shape with the ability to fit to a 1:1 kinetic model, further optimization of protocol and investigation of flow conditions is necessary before obtaining kinetic parameters. The irregular dips around 200s were due

to subtraction from mismatched injection cutoff times in the PBS sensor reference (black lines). Mass transport limitation due to protein aggregation was observed in Figure 10, as a dip in signal immediately before the association phase of NSB in 1% BSA.[32] The shape of mass transport limitation from sensor binding is carried over to the double-referenced WT binding curve (Figure 11) and masks the true specific Opa_{60}-nCEACAM1 response. Following previous SPR studies that found decrease in mass transport limitation while maintaining low NSB, combinations of lower BSA concentrations (minimum 0.1% w/v) and higher injection flow speeds will be used in the future.[32]

Once conditions have been optimized, the binding kinetics of the specific Opa_{60} HV region/GlcNAc-nCEACAM1 interaction will be determined by subtracting WT from HV- in addition to double-referencing. Although the K_D for Opa_{60} WT and GST-tagged nCEACAM1 has been characterized by Martin et al, SPR experiments will be used to obtain parameters for the Opa_{60} WT and HV-/GST-nCEACAM1 interaction to account for any differences in binding conditions. This comparison will ultimately be used to determine how different modifications of CEACAM1 (i.e. glycosylation) affect its ability to engage Opa_{60} and inform *in vitro* binding studies of their interaction.

6. Conclusion

Preliminary screening for evidence of the specific interaction between Opa_{60} and GlcNAc-nCEACAM1 in optimized conditions gave promising results for a single concentration of GlcNAc-nCEACAM1. So far, the most optimal regeneration was achieved using 1 M $MgCl_2$, and addition of BSA to PBS flow buffer reduced non-specific binding of GlcNAc-nCEACAM1 to the SA sensor. Specifically, BSA-containing flow buffer with immobilized Opa_{60} WT and nCEACAM1 injections demonstrates the expected response difference compared to Opa_{60} HV- and fits a 1:1 hyperbolic binding mode. However, further optimization and data points are needed in order to obtain accurate kinetic parameters to characterize the binding events. Future experiments with non-glycosylated nCEACAM1 will help reveal the effect of minimal N-glycosylation of nCEACAM1 on its Opa-binding capacity and will give confidence to *in vitro* investigations into the mechanism of Opa_{60}-CEACAM1 binding.

7. Acknowledgements

I owe all of the work presented here and beyond to Dr. Linda Columbus, who has been a caring mentor not only in research and academics but also in my personal life. Thank you for all your support and allowing me to pursue my own project on Opa-CEACAM.

Thank you to all members of the Columbus lab – Marissa Kieber, Jason Kuhn, Steven Keller, Nicole Swope, and Tracy Caldwell – for their guidance, discussions, and friendship, and to the Mura lab and Dr. Carol Price for their support. Special thanks to my graduate student mentor Marissa for training me and for being a wonderful mentor for the past three years. Thank you Tracy for help with SPR and edits. Thank you especially to Nicole for late-night discussions and for graciously offering moral and technical support when I most needed it.

This project was made possible by support from the University of Virginia Department of Chemistry, the UVA Harrison Undergraduate Research Award, UVA Ingrassia Research Grant, and NIH Grant R01 GB10204.

8. References

1. Tapsall, J. W.; Ndowa, F.; Lewis, D. A.; Unemo, M. *Expert Review of Anti-infective Therapy*. **2014**, *7*(7): 821-834.
2. World Health Organization (WHO), Department of Reproductive Health and Research. Emergence of multi-drug resistant Neisseria gonorrhoeae - threat of global rise in untreatable sexually transmitted infections, 2011, 2.
3. Grassme, H.; Gulbins, E.; Brenner, B.; Ferlinz, K.; Sandhoff, K.; Harzer, K.; Lang, F.; Meyer, T. F. *Cell*. **1997**, *91*(5): 605-15.
4. Dehio, C.; Gray-Owen, S. D.; Meyer, T. F. *Cell*. **1998**, *6*(12): 489-495.
5. Al-Jamal, W.; Kostarelos, K. *Accnt. Chem. Research*. **2011**, *44*(10):1094-1104.
6. Jolck, R. I.; Feldborg, L. N.; Andersen, S.; Moghimi, S. M.; Andresen, T. L. *Adv. BIochem. Eng. Biotechnol*. **2011**, *125*:251-80.
7. Hopfner, M.; Rothe, U.; Bendas, G. *J. Liposom Research*. **2008**. 18(1): 71-82.
8. Fox, D. A.; Larsson, P.; Lo, R. H.; Kroncke, B. M.; Kasson, P. M.; Columbus, L. *J. Am. Chem. Soc.* **2014**, *136*: 9938-9946.
9. Klaile, E. et al. The CEACAM1 N-terminal Ig domain mediates cis- and trans-binding and is essential for allosteric rearrangements of CEACAM1 microclusters
10. Bos, M. P.; Kao, D.; Hogan, D. M.; Grant, C. C.; Belland, R. *J. Infect. Immun*. **2002**, *70*, 1715.
11. Grant, C. C.; Bos, M. P.; Belland, R. *J. Mol. Microbiol*. **1999**, *32*: 233.
12. Virji, M.; Evans, D.; Hadfield, A.; Grunert, F.; Teixeira, A. M.; Watt, S. M. *Mol. Microbiol*. **1999**, *34*: 538.
13. Bonsor, D. A.; Gunther, S.; Beadenkopf, R.; Beckett, D.; Sundberg, E. J. *PNAS*. **2015**, *112*(44): 13561-13566.
14. Fedarovich, A.; Tomberg, J.; Nicholas, R.A.; Davies, C. *Acta Crystallogr.,Sect.D*. **2006**, *62*: 971-979.
15. Huang, Y.H.; Zhu, C.; Kondo, Y.; Anderson, A.C.; Gandhi, A.K.; Russell, A.; Dougan, S.K., Petersen, B.S., Melum, E., Pertel, T., Clayton, K.L., Raab, M., Chen, Q., Beauchemin, N., Yazaki, P.J., Pyzik, M., Ostrowski, M.A., Glickman, J.N., Rudd, C.E., Ploegh, H.L., Franke, A., Petsko, G.A., Kuchroo, V.K., Blumberg, R.S. *Nature*. **2015**, *517*: 386-390.
16. Martin, J. N.; Louise M. Ball, L. M.; Solomon, T. L.; Dewald, A. H.; Criss, A. K.; Columbus, L. *Biochemistry*. **2016**, *55*(31): 4286–4294.
17. Zhuo, Y.; Yang, J. Y.; Moremen, K. W.; Prestegard, J. H. *J. Biol. Chem*. **2016**, *291*(38): 20085–20095.
18. Daghestani, H.N. and Day, B.W. *Sensors*. **2010**, *10*: 9630-9646.
19. Liang, H.; Tuppurainen, J. P.; Lehtinen, J.; Viitala, T.; Yliperttula, M. Eur. J. Pharm. Sci. **2013**, *50*(3-4):492-501
20. Novotny, L.; Hecht, B. Principles of Nano-Optics; Cambridge University Press: Cambridge, UK, **2006**, 378-393.
21. Kimple, A. J.; Muller, R. E.; Siderovski, D. P.; Willard, F. S. Methods. Mol. Biol., 2010, 627, 91.
22. Johnsson, B.; Löfås, S.; Lindquist, G. Anal. Biochem., 1991, 198, 268.
23. Ferner-Ortner, J.; Mader, C.; Ilk, N.; Sleytr, U. B.; Egelseer, E. M. J. Bacteriol., 2007, 189, 7152.
24. Green, N. M. Methods Enzymol., 1990, 184, 51.
25. Holmberg, A.; Blomstergren, A.; Nord, O.; Lukacs, M.; Lundeberg, J.; Uhlén, M. Electrophoresis, 2005, 26, 501.
26. Pogoutse, A. K.; Lai, C. C.; Ostan, N.; Yu, R. H.; Schryvers, A. B.; Moraes, T.F. Analytical Biochemistry, 2016, 501, 35.
27. Haes, A. J.; Van Duyne, R. P. *Anal. Bioanal. Chem*. **2004**, *379*: 920–930
28. Wessels, H.; Paschke-Kratzin, A. *BIO Web of Conferences*. 2016, 7: 04002.
29. Granqvist, N.; Hanning, A.; Eng, L.; Tuppurainen, J.; Viitala, T. *Sensors (Basel)*. **2013**, *13*(11): 15348-15363.
30. Nicoya Lifesciences. How is LSPR Different from SPR? https://nicoyalife.com/technology/surface-plasmon-resonance/localized-surface-plasmon-resonance-theory (accessed April 9, 2018).
31. Dewald, A. H.; Hodges, J. C.; Columbus, L. *Biophys. J*. **2011**, *100*: 2131−2140.
32. Anggayasti, W. L. et al. Analytical Biochemistry. 2016, 499:43-50.
33. Anderluh, G.; Besenicar, M.; Kladnik, A.; lakey, J. H.; Macek, P. *Anal. Biochem*. **2005**, *344*: 43-52.

34. Baptista, A. L.; Coutinho, P. J>; Real Oliverira, M. E.; Rocha Gomes, J. I. *J. Liposome Research.* **2008**, *10*: 419-429.
35. Joguparthi, V.; Feng, S.; Anderson, B. *Int. J. Pharm.* **2008**, *352*(1-2): 17-28.
36. Biacore: Sensor Surface Handbook. GE Healthcare Bio-Sciences AB: Uppsala, Sweden. **2005**, 65-78.

10. Supplemental Figures

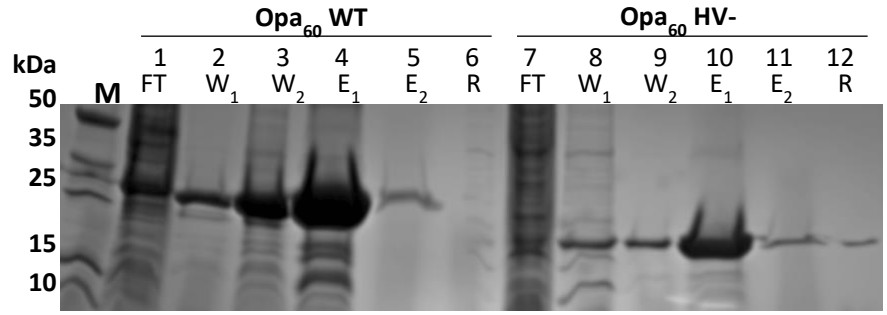

Figure 1. Recombinant Opa_{60} WT (MW = 30.89 kDa) and HV (MW = 22.49 kDa) protein preparation. SDS-PAGE of Co^{2+}-IMAC purification fractions against MW standard (Promega): flow-through (FT), wash (W), and elution (E) fractions of WT (30.89 kDa, lanes 1–5) and HV- (22.49 kDa, lanes 6-10).

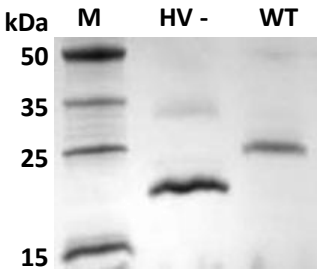

Figure 2. SDS-PAGE of folded Opa_{60} HV-less mutant (HV-, MW = 22.49 kDa) and wildtype (WT, MW = 30.89 kDa) after folding. Apparent MW is slightly lower than the actual MW due to condensed size.

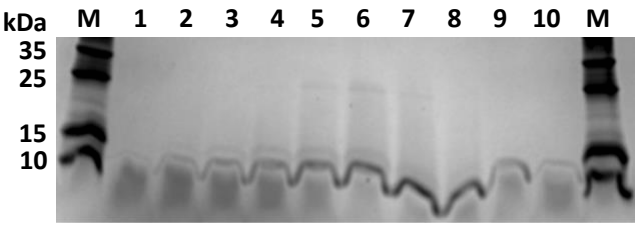

Figure 3. SDS-PAGE of GlcNAc-nCEACAM (12.88 kDa) fractions separated by FPLC. Fractions such as those in lanes 5-7 containing GFP (27 kDa) were pooled, re-dialyzed, and purified a second time using Co^{2+}-IMAC.

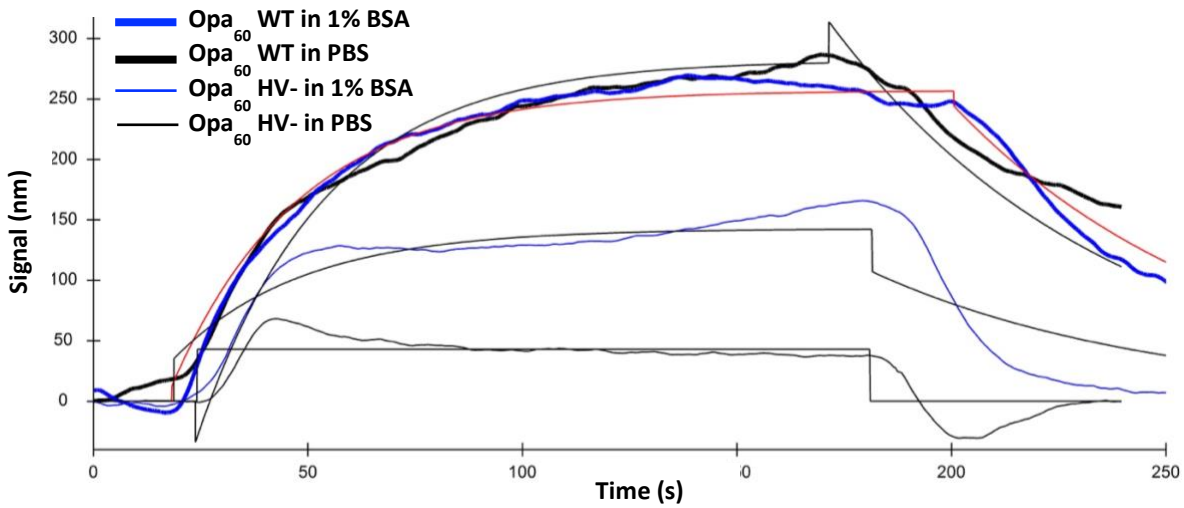

Figure 4. Fitting of Opa_{60}/GlcNAc-nCEACAM1 binding curves to a 1:1 binding model. Only Opa_{60} WT in 1% BSA loosely fit a 1:1 model, in red, after double-referencing sensor and flow buffer injection signals.